Smooth Cascade of Wrinkles at the Edge of a Floating Elastic Film

Jiangshui Huang,[1,2] Benny Davidovitch,[1] Christian D. Santangelo,[1] Thomas P. Russell,[2] and Narayanan Menon[1]

[1]*Department of Physics, University of Massachusetts, Amherst, Massachusetts 01003, USA*

[2]*Polymer Science and Engineering Department, University of Massachusetts, Amherst, Massachusetts 01003, USA*

(Received 26 October 2009; revised manuscript received 19 May 2010; published 14 July 2010)

An ultrathin polymer sheet floating on a fluid forms a periodic pattern of parallel wrinkles when subjected to uniaxial compression. The wave number of the wrinkle pattern increases sharply near the fluid meniscus where the translational symmetry of this one-dimensional corrugated profile is broken. We show that the observed multiscale morphology is controlled by a new ''softness'' number that quantifies the relative strength of capillary forces at the edge and the rigidity of the bulk pattern. We discover a new elastic cascade by which the wrinkling pattern in the bulk is smoothly matched to the fine structure at the edge by a discrete series of higher Fourier modes.

DOI: 10.1103/PhysRevLett.105.038302 PACS numbers: 82.35.Gh, 81.05.Lg, 83.10.Pp, 83.10.Rs

The translational symmetry of any patterned state is broken by a phase boundary, or a domain or sample wall. In condensed matter systems, the mechanism by which the pattern in the bulk matches up with the boundary has been addressed in the context of Landau branching in type-I superconductors [1] and the refinement of magnetic domains near grain boundaries [2]. We discuss this general problem in the context of a thin sheet that is decorated by a pattern generated by an elastic instability, and present a new mechanism by which an undulating shape in the bulk phase smoothly accommodates the tendency of the boundary to be flat, rather than by localized branching.

When a thin rectangular sheet floating on the surface of a pool of liquid is compressed along two opposing sides, it forms a pattern of parallel wrinkles, as shown in Fig. 1(a). Unlike the Euler buckling of an unsupported sheet, where the largest possible wavelength is selected, these wrinkles form at a wavelength $\lambda \ll W$, the width of the rectangle in the direction of the compression. However, Fig. 1 shows another striking phenomenon: the coarser pattern in the bulk gives way to a finer structure of wrinkles near the uncompressed edge. It is this cascade to ever-higher wave numbers that we examine in this Letter.

We performed controlled experiments with polystyrene (PS) sheets with typical lateral dimensions of $W \times L = 3 \times 2$ cm and thickness t between 50 and 400 nm. The sheets are prepared from PS solutions (atactic, number-average mol. wt. $M_n = 121$ K, weight-average mol. wt. $M_w = 1.05M_n$, radius of gyration $R_g \approx 10$ nm) in toluene, spin coated on to glass substrates. The thickness t was measured by x-ray reflectivity (Panalytical X-Pert diffractometer) with a precision of ± 0.5 nm. A rectangle was scribed onto the film with a sharp edge [3]. When the substrate was dipped into a petri dish of distilled, deionized water, the rectangle detached from the substrate. Since PS is hydrophobic, the film remained floating on the water, stretched out by the liquid-vapor surface tension, γ.

Two principles determine the bulk pattern: first, a thin sheet can be approximated as inextensible, so that the length of a line in the compression direction is preserved. Consequently, the wavelength and amplitude of the wrinkles are proportional. Second, the bending energy of the sheet favors long wavelengths (large amplitudes) whereas the gravitational energy of the liquid subphase favors small amplitudes (small wavelengths). Thus, the wavelength is selected by a compromise [4] between the bending and gravitational energies.

As shown in Fig. 1, when the sheet is compressed by a distance Δ (such that $\tilde{\Delta} \equiv \Delta/W \ll 1$), parallel wrinkles develop in the bulk. This one-dimensional pattern of wrinkles, characterized by a height field $\zeta(y)$ has for small amplitudes an energy per unit surface area

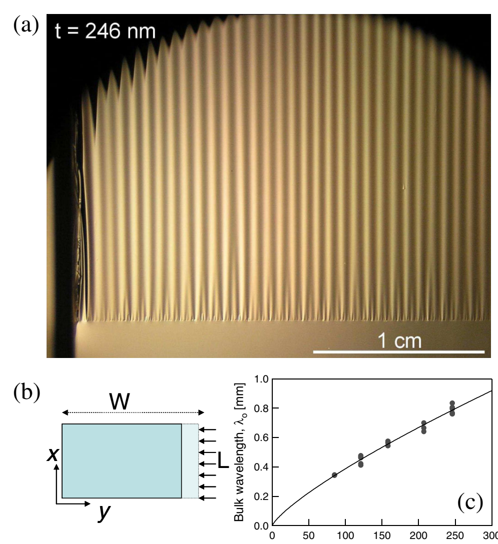

FIG. 1 (color online). (a) Image of a wrinkled PS sheet floating on the surface of water, compressed between two razor blades. (b) Sketch of geometry. (c) Bulk wavelength of wrinkles, $\lambda = 2\pi/q_o$ as a function of film thickness, t. The solid line is a fit to $t^{3/4}$, in agreement with the prediction of $q_o = (\rho g/B)^{1/4}$.

$$u = \frac{1}{2}\left(B\left(\frac{\partial^2 \zeta}{\partial^2 y}\right)^2 + \rho g \zeta^2 + \sigma\left[\left(\frac{\partial \zeta}{\partial y}\right)^2 - 2\tilde{\Delta}\right]\right). \quad (1)$$

The first two terms represent bending energy of the sheet and gravitational energy of the fluid, respectively. The third term enforces the constraint of inextensibility for small amplitudes, with the Lagrange multiplier σ being the stress σ_{yy} applied at the compressed edges. ρ is the density of the fluid, and the bending modulus is $B = Et^3/[12(1 - \Lambda^2)]$ [5], where E is Young's modulus and Λ is the Poisson ratio. The surface tension is absent from (1) because the bulk pattern has translational symmetry in the $\hat{x}$ direction. However, it is important to note that the sheet is still under a tension $\sigma_{xx} \approx \gamma$. Minimizing $u[\zeta]$ leads to a pattern

$$\zeta(y) = \frac{2}{q}\sqrt{\tilde{\Delta}}\sin(qy); \quad (2a)$$

$$\sigma_{yy} = (Bq^2 + \rho g/q^2), \quad (2b)$$

where the wave number $q = q_o = (\rho g/B)^{1/4}$ and $\sigma_{yy} = -2\sqrt{B\rho g}$. As shown in Fig. 1, this correctly describes the scaling of the wavelength of the wrinkles in the bulk. This scaling has been experimentally tested [6,7], and more broadly applied in situations where the bending energy is balanced by substrate elasticity [8], capillary forces [9], and tensile pre-stress [10].

We now turn to the main topic of this article, viz., the cascade approaching the edge. In Fig. 2(a), we show for PS films with $t = 85$ to 246 nm, the increase in wave number $q(x)$ as a function of distance x from the edge. Since $B \sim t^3$, this represents a broad range of B. For all thicknesses, $q(x)$ increases to a value q_e at the edge, that is 2 to 5 times larger than the bulk value q_o. The evolution to higher wave numbers occurs over approximately the same distance from the edge: though an exponential fit shows systematic deviations, such a fit estimates the penetration length of the edge into the bulk to be 1.8 ± 0.2 mm.

Intuitively, a higher wave number at the edge is to be expected. The fluid meniscus follows the contour of the edge of the sheet. To minimize the surface energy of the air-water interface it is favorable to reduce the amplitude of the wrinkles at the edge. In order to preserve inextensibility, the wave number increases. This cascade to finer wrinkles terminates at a wave number, q_e, where the gain in surface energy is offset by the increased cost of bending. Notwithstanding these plausible arguments, previous experiments in this geometry [6] did not show a marked effect at the boundary, and found that $q_e \approx q_o$. We thus need to address some obvious issues: What are the relevant parameters that dictate whether a cascade appears? What governs the amplification of the bulk wavelength, and what is the length over which the cascade occurs?

In order to understand wave number amplification in our experiment, we estimate the energy cost of a wave number q_e at the edge. The capillary energy of an undulated meniscus of wave number q_e and amplitude ζ_e is: $U_{\rm cap} = (1/2)\gamma\zeta_e^2\sqrt{(\rho g/\gamma) + q_e^2} = 2\gamma(\tilde{\Delta}/q_e^2)\sqrt{(\rho g/\gamma) + q_e^2}$

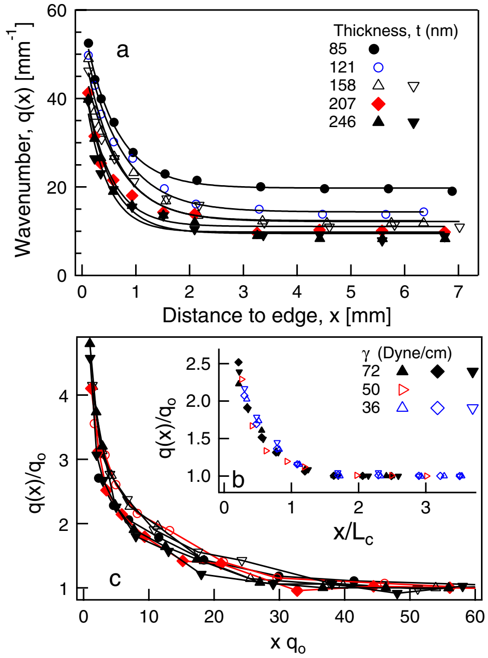

FIG. 2 (color online). (a) Wave number $q(x)$ as a function of distance x from the edge of the sheet. The length scale over which the decay occurs does not change strongly with thickness t of the sheet. Exponential fits (solid lines) to $q(x)$ deviate from the data but yield a decay length of 1.8 ± 0.2 mm. (b) $q(x)/q_o$ vs x/L_c, where $L_c = \sqrt{\gamma/\rho g}$. The data for three values of γ show good collapse. (c) The data of (a) with the scaled wave number $q(x)/q_o$ vs the scaled distance from the edge xq_o. Data collapse is good at small and large xq_o, but is poor at intermediate distances indicating a multiscale evolution.

[where we use Eq. (2b)]. $U_{\rm cap}$, which is an energy per unit *length*, is a decreasing function of q_e, schematically plotted in Fig. 3(a). To compare it to the energy cost per unit *area* of the affected part of the sheet [Fig. 3(b)], we require the length scale l_p over which the pattern at the edge penetrates into the sheet.

This leads us to consider the energetic effect of breaking translational symmetry. The tension in the $\hat{x}$ direction is incorporated by modifying Eq. (1) to

$$u = \frac{1}{2}\left(B(\nabla^2\zeta)^2 + \rho g\zeta^2 + \gamma\left(\frac{\partial \zeta}{\partial x}\right)^2 + \sigma(x)\left[\left(\frac{\partial \zeta}{\partial y}\right)^2 - 2\tilde{\Delta}\right]\right). \quad (3)$$

The new term is the energy of the deformation in the $\hat{x}$

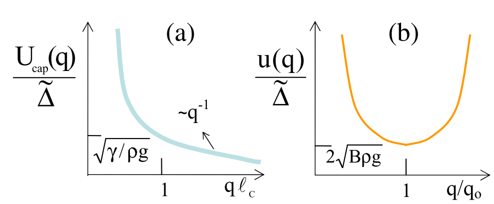

FIG. 3 (color online). (a) The energy per length of the meniscus, $U_{\rm cap}(q_e) = 2\gamma(\tilde{\Delta}/q_e^2)\sqrt{(\rho g/\gamma) + q_e^2}$. (b) Energy per area of a sheet with wave number q, $u(q) = (\tilde{\Delta}/q^2)B(q^4 + q_o^4)$.

direction under the interfacial tension γ. To estimate the penetration length l_p, we consider the superposition

$$\zeta(x, y) = \zeta_0(x)\cos(q_0 y) + \zeta_e(x)\cos(q_e y), \qquad (4)$$

and minimize (3) while preserving inextensibility along $\hat{y}$. When the compressive force in the y direction is much smaller than the tensile force in the x direction, $\varepsilon \equiv \sigma/\gamma \approx \sqrt{\rho g B}/\gamma \ll 1$, one finds [11] that the dominant energies are bending ($\frac{B}{2}(\frac{\partial^2\zeta}{\partial y^2})^2$) and tensile ($u_T = \frac{\gamma}{2}(\frac{\partial\zeta}{\partial x})^2$). From the balance $Bq_0^4 \sim \gamma l_p^{-2}$, we obtain $l_p \approx \sqrt{\gamma/\rho g}$, which is the capillary length, l_c. This is consistent both with the magnitude of the typical penetration length found in Fig. 2(a), and with its insensitivity to the thickness t. Notice that the stress ratio ε ranges between 6×10^{-4} and 3×10^{-3} in our experiments, thus validating the regime assumed in the foregoing argument. Furthermore, we performed experiments by adding a surfactant at various concentrations to the aqueous subphase, reducing γ by a factor of 2. The data collapse in Fig. 2(b) upon rescaling $x \to x/l_c$ validates this argument.

Using this estimate of the penetration length, l_p, we return to the wavelength amplification ratio q_e/q_0: the bending energy cost near the edge is $U_{\text{edge}} \sim l_p u(q_e) \sim l_c B\tilde{\Delta} q_e^2$. Setting the edge and meniscus energies to be comparable, $U_{\text{edge}} \sim U_{\text{cap}}$ we obtain $q_e \sim (\varepsilon)^{-1/6} q_0$. This argument shows that for $\varepsilon \ll 1$ (as in our experiments) the wave number amplification is a large effect. A similar argument shows that for $\epsilon \gg 1$ the edge effect is only a small perturbation to the bulk pattern, in agreement with [6]. However, the estimate $U_{\text{edge}} \sim q_e^2$ rests on the assumption of a single penetration length. This is an oversimplified picture as the cascade shown in Fig. 2 proceeds via a sequence of intermediate wave numbers. A full solution of the nonlinear problem [12] reveals that this instability results from a logarithmic dependence of $U_{\text{edge}} \sim \log q_e$, which lowers the energetic cost for sufficiently large q_e.

The cascade pattern is characterized by a hierarchy of wave numbers q_i intermediate between q_0 and q_e, each with a penetration length $l_p(q_i)$ characterizing the transitions between zones dominated by wave numbers q_i and q_{i+1}. These lengths range from $l_p \sim l_c$ for $q_i \to q_0$ to $l_p \sim q_e^{-1}$ for $q_i \to q_e$ [11]. This reflects an enhancement of the compression-tension ratio ε towards the edge, Eq. (2b), the compression increases with wave number as $\sigma(x) \sim Bq^2$. That the description in terms of a single penetration length l_p is simplified can be seen from Fig. 2(c), where we show the scaled wave number $q(x)/q_0$ vs xq_0, the scaled distance from the edge. This scaling yields good data collapse far from the edge, and even close to the edge. However, the data do not collapse in between, indicating a q-dependent penetration length $l_p(q)$.

Thus far, our analysis of the wave number amplification has shed no light on the nature of the cascade itself. A well-known example of an elastic cascade was constructed by Pomeau and Rica [13] for the "curtain geometry" of a tension-free sheet rippled under a compressive force but constrained to be flat at one edge. They showed that the matching of the ripples to the flat edge ($q_e \to \infty$) could be achieved by hierarchy of branching events, in which each wrinkle branches into a succession of sharp folds with flat faces.

One superficial difference between what we observe and the Pomeau-Rica cascade is that our cascade terminates at a finite wave number, and therefore passes through only a few generations. The more profound difference, as was pointed out in [12], stems from the fact that our sheets experience a tension along the uncompressed direction. Any deviation from a one-dimensional pattern imposes curvature in both directions; this Gaussian curvature generates in-plane stretching energy controlled by a modulus $Y = Et$. In the Pomeau-Rica scenario, in the absence of tension, the dominant contribution to the strain energy is the anharmonic energy density $u_G \sim Y\zeta_x^2\zeta_y^2$, whose minimization leads to localized Gaussian curvature along a sequence of sharp ridges [14]. However, the consequence of the applied tension is that the focusing of Gaussian curvature does not relieve the strain energy at other points: as noted in Eq. (3), the tension term u_T penalizes slope, and is nonzero even on flat facets where the Gaussian curvature vanishes. This mechanism thus favors a smooth reduction of the amplitude, which is accomplished by the superposition of a finite number of Fourier modes with distinct wave numbers. Smooth cascades can thus be expected if $u_T > u_G$ [15]. For $\tilde{\Delta} \ll 1$, this condition translates to small compression-tension ratio: $\varepsilon \lesssim 1$ [12]. In our experiments the value of $\varepsilon \ll 1$, indicating a novel, smooth hierarchy, markedly different from the Pomeau-Rica stress-focusing cascade.

A closer look at the cascade, as shown in the magnified view of Fig. 4(a), supports the scenario of a smooth mechanism in which larger amplitudes of higher wave-number Fourier components are smoothly mixed in as one approaches the edge. In Fig. 4(b) we present a more quantitative measure of the smoothness of the cascade. At a given distance x from the uncompressed edge we determine from the image, the separations d, between the crests of the wrinkles. At each value of x, we show a histogram of $q_o d/(2\pi)$, the normalized separation between wrinkles. Far away from the edge, the separations are all concentrated at $q_o d/(2\pi) = 1$. As expected, closer to the edge, more crests are formed, and at smaller values of d. Importantly, none of the histograms show significant weight near $d = 0$. In a scenario where wrinkles divide by localized branching, one might expect a preponderance of small values of d just after a branch point, between sibling branches of the same parent wrinkle. That appears not to be the case in Fig. 4, with separations flowing smoothly to a mixture of higher Fourier components.

The three forces operative in this problem—gravity, bending, and capillarity—can be combined in pairs to yield three distinct length scales: $(B/\rho g)^{1/4}$, $(B/\gamma)^{1/2}$,

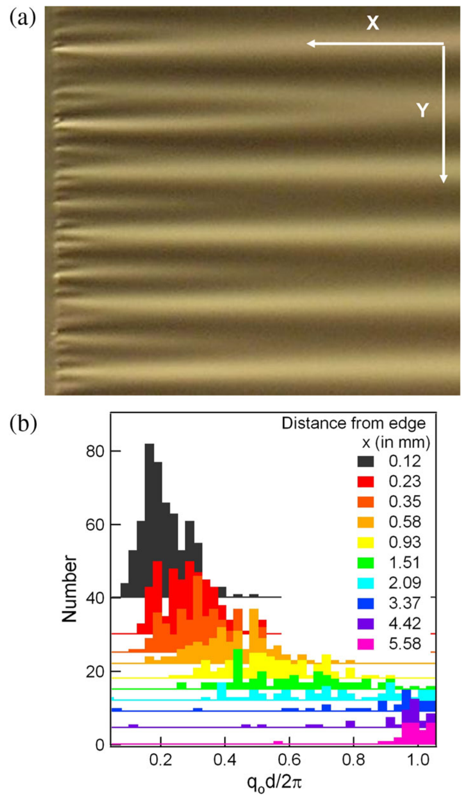

FIG. 4 (color online). (a) A magnified image of the cascade. (b) At each value of x, a histogram of the scaled separation, $q_o d/(2\pi)$, between crests, for several values of distance x from the edge. Data were collected from two films with $t = 246$ nm. The separations d, are determined from the locations of maxima of the intensity in the $\hat{y}$ direction.

and $l_c = (\gamma/\rho g)^{1/2}$. The first of these is q_o, the second, an elastocapillary length [17] which controls q_e, and the third is the capillary length, which determines the length of the cascade. However, the stress ratio $\varepsilon = \sigma/\gamma$ dictates the overall morphology of the pattern in our experiments. Surface tension plays a dual role in our experiments, determining both the energy of the fluid meniscus, U_{cap}, as well as the tension applied in the uncompressed direction. In principle, these are different effects that could be independently tuned. Increasing the capillary energy cost of the edge can tune a transition from the regime of our experiment to that of stiffer sheets, in which the effect of the edge is small. On the other hand, decreasing the applied tension could drive a transition from the smooth, energy-delocalized cascades we observe, to a regime of localized branching [13] with energy focusing. Thus, our observations open the way to the exploration of a rich phase diagram of both branched and smooth structures [12], and possibly even flat, stretched boundary layers [16]. The relationship between the elastic cascades we observe and cascades in sheets with intrinsically non-Euclidean metrics [18] has yet to be uncovered. It also remains to be seen whether analogues of our smooth cascades may be found in other microstructured materials [1,2] where branching cascades have been observed.

We acknowledge support from the Center for University of Massachusetts Industry Cooperative Research Program (J. H.); the NSF MRSEC on Polymers at the University of Massachusetts; the U.S. DOE, through DE-FG-0296 ER45612 (T. P. R.); and NSF-DMR 0606216 (N. M.) and NSF-CBET-0609107 (T. P. R., N. M.). We thank B. Roman, E. Sharon, B. Audoly, A. Boudaoud, R. Kamien, and D. Nelson for useful conversations.

[1] A. Hubert and R. Schäfer, *Magnetic Domains: The Analysis of Magnetic Microstructures* (Springer, Heidelberg, 1998).
[2] R. P. Huebener, *Magnetic Flux Structures in Superconductors* (Springer, Heidelberg, 2001).
[3] To obtain extremely well-defined edges, in a few selected cases we spin-coated the film on an Si wafer with an SiO_2 surface layer. The wafer was fractured along a crystal plane, and the film lifted off with HF solution.
[4] E. Cerda and L. Mahadevan, Phys. Rev. Lett. **90**, 074302 (2003).
[5] L. D. Landau and L. M. Lifshitz, *Theory of Elasticity* (Pergamon, New York, 1986).
[6] L. Pocivavsek *et al.*, Science **320**, 912 (2008).
[7] D. Vella, P. Aussillous, and L. Mahadevan, Europhys. Lett. **68**, 212 (2004).
[8] C. M. Stafford *et al.*, Nature Mater. **3**, 545 (2004).
[9] J. Huang *et al.*, Science **317**, 650 (2007).
[10] E. Cerda, K. Ravi-Chander, and L. Mahadevan, Nature (London) **419**, 579 (2002).
[11] Minimization of the energy (3) with boundary conditions $\zeta_e(-\infty) = 0 = \zeta_q(0)$ yields nonlinear equations for ζ_q, ζ_e [12], whose solution yields the length $l_p(q)$.
[12] B. Davidovitch, Phys. Rev. E **80**, 025202(R) (2009).
[13] Y. Pomeau and S. Rica, C.R. Acad. Sci. Paris. **325**, 181 (1997).
[14] T. A. Witten, Rev. Mod. Phys. **79**, 643 (2007).
[15] Energetic upper bounds based on smooth cascades were derived [16] for the zero tension Pomeau-Rica problem, but the existence of a cascade of sharp folds has not been proven or ruled out.
[16] W. Jin and P. Sternberg, J. Math. Phys. (N.Y.) **42**, 192 (2001); H. B. Belgacem, S. Conti, A. DeSimone, and S. Műller, J. Math. Phys. (N.Y.) **10**, 661 (2000); B. Audoly and A. Boudaoud (private communication).
[17] J. Bico, B. Roman, L. Moulin, and A. Boudaoud, Nature (London) **432**, 690 (2004).
[18] E. Sharon *et al.*, Nature (London) **419**, 579 (2002); B. Audoly and A. Boudaoud, Phys. Rev. Lett. **91**, 086105 (2003).